Studies of the Luminous Hypersonic Wake

R. L. TAYLOR,* B. W. MELCHER II,† AND W. K. WASHBURN‡
Avco Corporation, Everett, Mass.

Measurements of the width of luminous wakes behind hypervelocity blunt bodies launched in ballistic ranges are presented. Experiments utilizing an image converter camera, a race track drum camera, and a photoelectric wake scanner have obtained data over 1200 body diameters of wake length on 0.22, 0.55, and 1.0-in.-spherical projectiles for freestream pressures from p_∞ = 0.2 to 10.0 cm Hg and projectile velocities from V_∞ = 12,000 to 20,500 fps. The results of the luminous wake width measurements are shown to agree well with the viscous core width data obtained with shadowgraph and schlieren techniques. It is found that the luminous wake growth has a pressure dependence in the transition and laminar flow regimes, but not in the turbulent regime from 2.0 to approximately 76 cm Hg. The turbulent experimental results are compared to the wake growth theories of Lees and Hromas and Lykoudis. The simple asymptotic turbulent wake growth correlation, $w/(C_DA)^{1/2} = K[x/(C_DA)^{1/2}]^{1/3}$, is shown to give good agreement with the data with K = 0.66. Finally, the occurrence of asymmetries in the wake is documented. The polarization of these asymmetries seems to add further observational evidence of the occurrence of large scale structure in the turbulent hypersonic wake.

I. Introduction

THE structure of the wake behind bodies traveling at hypersonic speeds in air is controlled by a complex interaction of aerodynamics and chemistry, with the added complexity of flows that may vary from laminar, unsteady, and periodic, to fully turbulent. Several attempts have been made to predict some of the gross features of the hypersonic wake such as the rate of growth of the inner viscous core or boundary-layer induced wake.[1–4] These theoretical predictions have been compared with measurements of the width of the turbulent viscous wake obtained in various ballistic range experiments.[5–9] All of the experimental measurements on wake width reported to date have utilized the schlieren or shadowgraph technique and, therefore, measure a region in the wake defined by density gradients. The sensitivity limit of these techniques has, until now, restricted their applicability to measurements of the unsteady or turbulent wake.

When plastic projectiles are fired at hypersonic velocities into a ballistic range, considerable ablation occurs and the wake becomes highly luminous.[10, 11] The ablation products may be thought of as a dye, which defines the viscous wake in much the same manner as dyes are used to delineate low-speed flow patterns.[12] If this assumption is correct, then the luminous wake seen in hypersonic experiments should correspond to the viscous wake. In the present investigation, these ablation products are used as an observable to define the width and rate of growth of the luminous viscous wake in both laminar and turbulent flow out to 1200 body diameters behind blunt bodies. Measurements were made on 0.22-in.-diam lexan spheres in the velocity range of 12,000 to 15,000 fps and on 0.55- and 1.0-in.-diam lexan spheres, unsaboted and saboted, respectively, fired at the Canadian Armament Research and Development Establishment (CARDE), Valcartier, Quebec, Canada, at velocities of 15,000 to 20,500 fps. The measurements were made over a range of freestream pressure of 0.2 to 10.0 cm Hg of air.

Three experimental techniques have been employed in the present study: an image converter camera used to photograph the near wake region out to 10 body diameters downstream, a racetrack technique used from 7 to 100 body diameters, and a wake scanner instrument used to measure the width of the luminous wake out to 1200 body diameters.

II. Experimental Techniques and Data

Image Converter Camera

Near the body where the radiation intensities are the highest, a snapshot technique may be used to photograph the luminous flow field provided that fast shuttering is available to stop the motion. The image converter camera[13] is an instrument in which fast electronic shuttering plus a limited, amount of light amplification are available, and, therefore, it is ideally suited to photographing the base and near wake region.[11, 14, 15] The instrument§ used in this study employs an RCA tube with S-11 spectral response and has a light gain of about 50 from the photocathode to the photoanode. A framing unit is used which allows three consecutive exposures to be made with preset time intervals between frames. Figure 1a illustrates a typical image converter photograph of a 0.22-in.-diam lexan sphere fired into air. The exposure conditions are given in the caption. Considerable detail of the luminous flow field around the body and in the base region out to about 10 body diameters is evident. By calibrating this camera against a known scale, it is possible to measure the dimensions of the luminous wake from such a photograph. Figure 1b shows reduced width data of the luminous wake w plotted against distance downstream of the projectile x, both normalized by the body diameter d. The

Presented as Preprint 64-45 at the AIAA Aerospace Sciences Meeting, New York, January 20–22, 1964; revision received June 15, 1964. Supported jointly by Ballistic Systems Division, U. S. Air Force under Contract No. AF 04(694)-33 and Advanced Research Projects Agency, as monitored by the Army Missile Command under Contract No. DA-19-020-ORD-5476 (part of Project Defender). The cooperation and assistance of George Tidy, Superintendent, Aerophysics Wing; André Lemay, Head, Radiation Physics Section; and the staff of the Canadian Armament Research and Development Establishment is gratefully acknowledged. Melvin Shakun contributed to the curve fitting procedures. The data gathering and data analysis were under the direction of Robert McMillen and Victor Oppenheimer, respectively.

* Principal Research Scientist, Avco-Everett Research Laboratory.

† Now at National Engineering Science Company, Pasadena, Calif. Member AIAA.

‡ Senior Engineer, Avco-Everett Research Laboratory. Member AIAA.

§ Model C image converter camera manufactured by STL Products, Inc., Los Angeles, Calif.

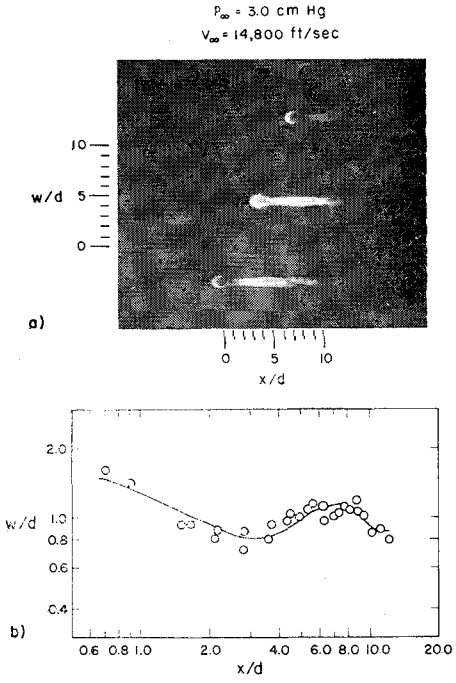

Fig. 1 a) Image converter photograph of the base flow region of a 0.22 in.-diam lexan sphere fired into air. There are three frames per picture. The time sequence runs from top to bottom as the projectile moves from right to left. The camera conditions are: lens, f/2; exposure, 0.2 μsec; and time between frames, 5 μsec. b) Reduced width data w/d plotted against distance downstream, x/d, from the image converter photograph in a.

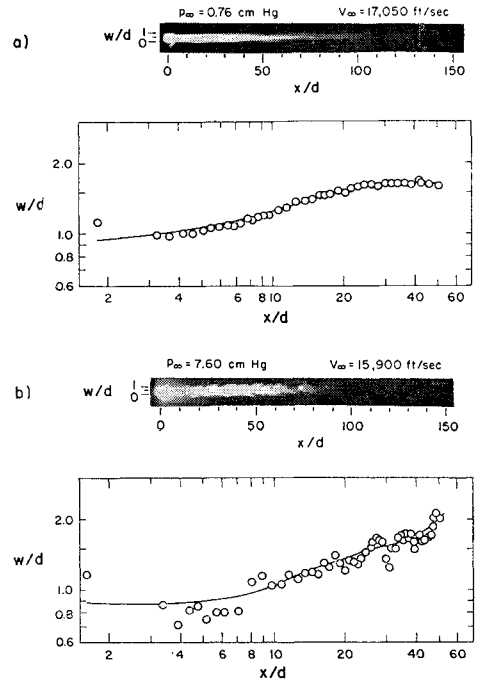

Fig. 2 Race track photographs of the luminous hypersonic wake behind the 0.55-in.-diam spherical body fired into air. a) representative of the unsteady wake near the transition to laminar flow; and b) fully turbulent luminous wake. The luminous wake growth data obtained from these photographs are plotted beneath each race track picture.

solid curve is a quartic, least-squares-fit to the data. Around the projectile, it can be seen that the luminous wake width is considerably larger than the body, indicating that in this region there may be a contribution of inviscid gas to the luminous wake. Also in this region of the flow field, the radiation intensity is the highest, and overexposure could be contributing to the wake width. The luminous wake contracts in the base flow region producing a minimum width of about 0.8 diam at 3 to 4 x/d downstream. Then the wake begins to expand. At about 8 to 10 x/d, the luminous wake again appears to contract as the intensity of the wake falls below the sensitivity of the instrument. Vignetting of the image by the instrument also contributes to the rapid extinction of the luminous wake. The experimental conditions employed in this study with the image converter camera are shown in Table 1. Useful wake widths were generally obtained out to about 10 x/d.

Race Track Technique

Further downstream in the wake where the temperatures are lower, and therefore the radiation considerably less intense, techniques with higher effective exposures must be used to photograph the wake. The race track flow visualization technique[16, 17] is one such method. A portion of luminous wake is tracked by film on a rotating drum as the event traverses a vertical slit placed between the wake and the drum camera. Since the motion of the wake is primarily one-dimensional, the exposure level on the film can be increased by tracking without sacrificing resolution.

Table 1 Experimental conditions

Instrument	p_∞, cm Hg	V_∞, kft/sec	d, in.	Sabot
Image Converter	2–10	12–15	0.22	No
Race track	0.6–10	16–20.5	0.55	No
	0.76–7.6	15–16	1.0	Yes
Wake scanner	0.2–10	16–20.5	0.55	No

Examples of photographs of the self-luminous wake taken by this method are shown in Figs. 2a and 2b for firings of 1.0-in.-diam. spheres into air. In this data, the drum speed was set to track the wake in the expansion controlled region causing mistracking and loss of detail in the base and near wake region ($x/d < 7$). Also, the radiation intensity around the projectile is sufficiently high so that the film is overexposed for several body diameters. Because of this mistracking and overexposure, the race track data reported herein are not useful at distances less than 7 x/d downstream in the wake. In interpreting these photographs, it is important to realize that they are not snapshots. Since different parts of the photograph are exposed at different times, a distortion results in which the apparent distance from the body is shortened, although the local structure of those events that are being tracked is correctly reproduced. It has been calculated from experimental data on wake velocity[10] that a mistracking error of about 5% in x/d can occur in the region, 7 to 100 x/d, because of the wake velocity varying from an assumed constant value. The interpretation and reduction of race track pictures have been thoroughly discussed by Washburn and Keck.[16]

Wake widths measured from the race track photographs are shown below each picture in Figs. 2a and 2b, together with quartic, least-squares curves fits to the data. It is to be noted that in Fig. 2a the width of the wake begins to decrease at about 50 x/d as the sensitivity limit of the technique begins to be approached. The race track technique has been used to obtain width and growth data for luminous wakes from about 7 to 100 body diameters for the experimental conditions given in Table 1. Data covering the range between fully turbulent and unsteady wakes have been obtained, i.e., Figs. 2a and 2b. By using two race track instruments that are arranged orthogonal to each other on the ballistic range, it also has been possible to study the symmetry of the luminous wake.

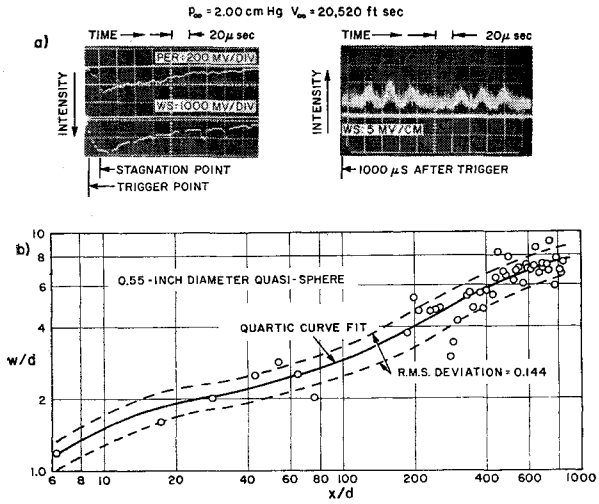

Fig. 3 a) Wake scanner oscillograph records of the luminous wake width for a 0.55-in.-diam spherical body fired into air. The reduced data obtained from these pictures are plotted beneath the oscillographs in b.

Wake Scanner

In order to study the luminous wake further downstream where the race track method is not sufficiently sensitive, a photoelectric instrument, the wake scanner, was devised.[18] This instrument utilizes a six-faced rotating mirror, a set of up to 17 fixed apertures, and a photomultiplier tube to measure the radiation intensity from a small volume element that is repetitively scanned in a vertical direction across the wake. The spatial resolution and scanning frequency can be widely varied and are controlled by a combination of optical parameters of the instrument and rotational velocity of the mirror. Under optimum conditions, resolution of a small fraction of a body diameter is possible with repetitive scans every few body diameters in the wake.

Sample data from the wake scanner are shown in Fig. 3a for the firing of a 0.55-in.-diam lexan sphere into air. In Fig. 3a, the upper beam of the oscillogram, labeled *PER*, is a time mark; the downward deflection of this beam just after triggering indicates the passage of the stagnation point of the model by the instrument location. The lower beam on this oscillogram, labeled *WS*, is the signal from the scanner. Radiation profiles are obtained about every 17 μsec, corresponding to about every 6 body diameters in the wake. The right-hand oscillogram shows a section of data recorded more than a millisecond or more than 500 body diameters after the projectile passage and demonstrates the capability of the instrument to record luminosity in the far wake. Figure 3b shows reduced wake scanner width data for this round as a function of distance downstream in the wake. In the near wake, at less than 10 x/d, the present wake-scanner measurements are not too reliable as a width measurement because of a large background signal; the sensitivity of the instrument has been intentionally set high in order to make observations in the far wake. The wake scanner has provided profiles of the radiation history of the wake up to 1200 body diameters downstream of the model for the flight conditions listed in Table 1. This flight regime covers a range of Reynolds number which encompasses laminar, unsteady, and turbulent wakes.[9]

Accuracy and Presentation¶ of Data

As just indicated, these experimental techniques have certain regions of applicability defined either by their inherent sensitivity or by the manner in which they were operated in the current study. Within these regions of applicability, the estimated precision of the over-all measurements are summarized in Table 2.

¶ More details on this section may be found in Ref. 19.

Table 2 Precision of measurements

	w/d, %	x/d, %
Image converter	±14	±14
Race track camera	±10	±11
Wake scanner	± 8	± 6

The data on the width of the luminous wake have been analyzed in this paper in terms of equivalent drag area, i.e., nondimensionalized by $(C_DA)^{1/2}$. It is realized that the wake growth data presented here does not extend far into the asymptotic growth region of the wake where $(C_DA)^{1/2}$ is most properly justified as the correlating parameter. Also, for the projectiles employed in this study, there is insufficient variation in $(C_DA)^{1/2}$ to establish its validity as a scaling parameter. However, for consistency with other published work,[20] and considering the physical significance of this parameter from momentum considerations, it is used here as the scaling parameter. For spheres, $(C_DA)^{1/2} \simeq 0.89\ d$, and use of the body diameter as a scaling parameter introduces only small variations from the present results.

In the present study, two of the projectiles, the 0.22- and 1.0-in. diam, were spheres. The other model, a 0.55-in.-diam quasi-sphere, is shown in cross section in Fig. 4a. This axisymmetric body has a spherical nose and a cylindrical body with flare that is supposed to shear off during launch. The dimensions shown in Fig. 4a are for the body before launch; significant deformations were observed during flight as shown by the shadowgraph in Fig. 4b. The drag coefficient for this body was calculated from Newtonian theory for the actual shapes observed in shadowgraph pictures that were taken on each run to observe projectile integrity, attitude, and velocity. The variation of C_D with θ_T is shown in Fig. 4c. Also shown are the average and extreme values of θ_T measured from shadowgraphs and the values of θ_T before launching. As can be noted, the value of C_D calculated from the shadowgraphs is within a few percent of $C_D = 1.28$ which makes $(C_DA)^{1/2} = d$. For convenience, this was the

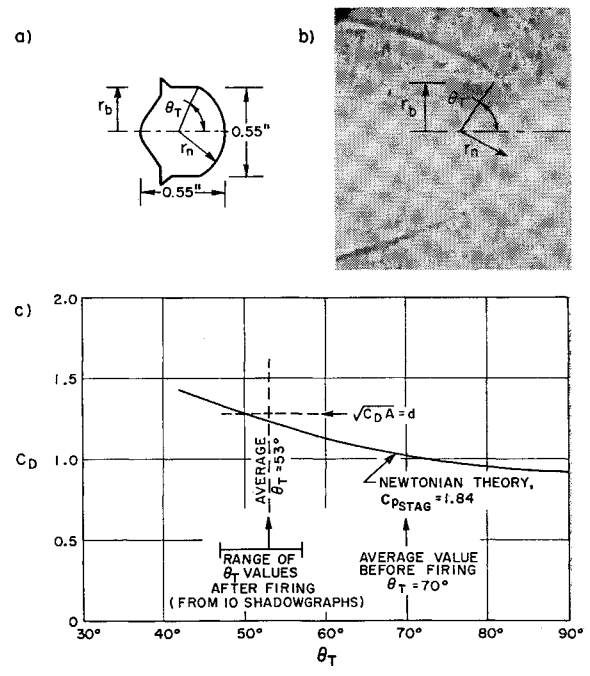

Fig. 4 Quasi-sphere geometry and in-flight drag estimation. a) The projectile before launching; b) a shadowgraph of the projectile in flight showing some distortion; c) the calculated drag coefficient, C_D vs. θt.

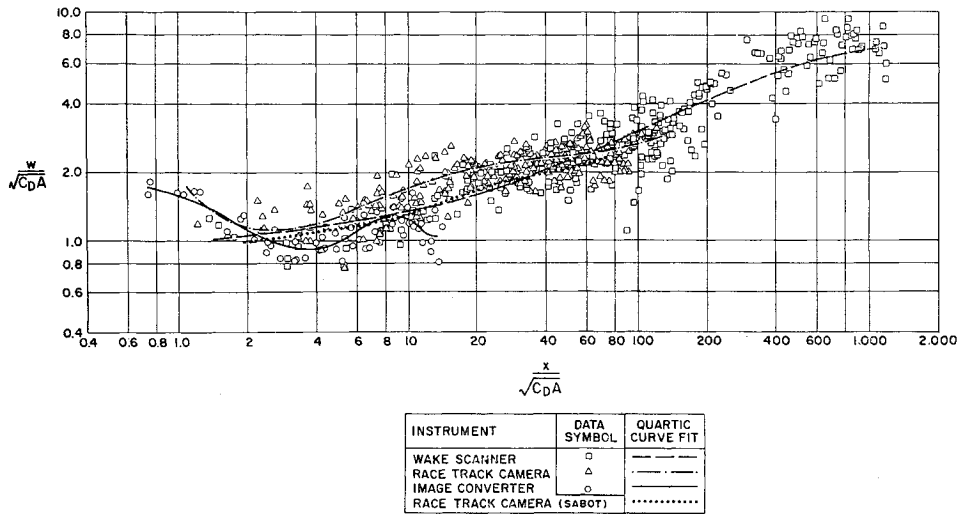

Fig. 5 Comparison of the luminous wake width data obtained by the wake scanner, race track, and the image converter camera. The experimental conditions for these data are given in Table 1.

value of C_D used in the data reduction for the 0.55-in. quasi-sphere.

To facilitate presentation, analysis, and discussion, the data were fit to a fourth-degree polynomial by the method of least squares. The quartic polynomial has the advantage of having well-known curve fit solutions and computer programs. The quartic fit was made to the logarithms of the data for two reasons. First, studies indicate that the statistical distribution of the deviations in the data were more nearly normal in the logarithmic form as compared to the algebraic form. Secondly, the effect of the preponderance of data points at the high values of the radial and axial coordinates were lessened by the logarithmic polynomial form.

III. Results

Comparison of Techniques

Data obtained with the three experimental techniques are compared in Fig. 5. For each of the three instruments, the figure shows sample data and the quartic curve fit to that data. This figure was prepared from 77 rounds with free-stream pressures $1.9 \leq p_\infty(C_DA)^{1/2} \leq 17.1$ cm Hg-cm. Experimental data are presented in a following section which indicate that in this pressure regime, where the wake is fully turbulent, the width measurements are independent of ambient pressure effects. In Fig. 5, only a sample of about 300 data points out of a total of almost 3500 have been plotted for illustration. These points represent a sample of all the data and are not necessarily restricted to the previously discussed regions of applicability of the various techniques.

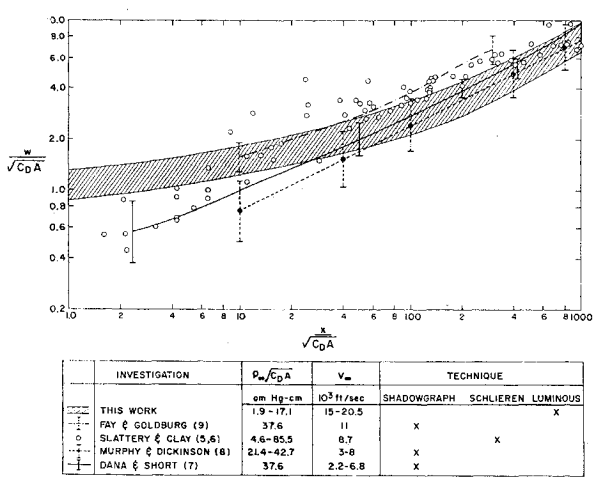

Fig. 6 Combined luminous wake width data compared with shadowgraph and schlieren measurements. The luminous wake width data are presented as the rms band (shaded area) to the quartic fit of the data.

It is apparent from Fig. 5 that the three measurement techniques provide consistent results within the fluctuations of the data and the regions of overlapping coverages and applicability. The image converter camera is effective in the base region and near wake where the race track camera is subject to mistracking and overexposure and where the wake scanner traces are difficult to interpret because of the high background signal. Beyond the region of applicability of the image converter $x/(C_DA)^{1/2} \geq 10$, the race track provides clear definition of the luminous wake width out to about 100 $x/(C_DA)^{1/2}$. The wake-scanner data are generally valid for $x/(C_DA)^{1/2} \gtrsim 10$ and extend to beyond 1200 $x/(C_DA)^{1/2}$. The differences between the wake scanner and the race track camera results in the region $7 \leq x/(C_DA)^{1/2} \leq 30$ is believed to be interpretive in nature.[19]

Comparison with Other Wake Width Measurements

The results of the present investigation are compared with other experimental results in Fig. 6. The luminous wake growth curve shown in this figure is the envelope of the rms deviation to the composite quartic fit to all the image converter, race track camera, and wake-scanner data presented in Fig. 5. The other results presented are shadowgraph and schlieren measurements of the viscous core of the wake and were obtained at the $p_\infty(C_DA)^{1/2}$ values indicated on the figure. Shown are the quartic fit and rms deviation to the shadowgraph data of Fay and Goldburg[9] taken at 1-atm pressure for a 0.22-in.-diam sphere, the data points from schlieren studies of Slattery and Clay[5, 6] for the 0.25- and 0.50-in.-diam spheres at 4.1 to 76 cm Hg, a median line and envelope to the shadowgraph data of Murphy and Dickinson for 0.125- and 0.25-in.-diam spheres at 1 atm, and the average curve and spread of the shadowgraph data of Dana and Short for a 0.22-in.-diam sphere fired into 1 atm. Beyond $x/(C_DA)^{1/2} \approx 7$ and to the limits of the data [$x/(C_DA)^{1/2} \simeq 1200$], the luminous wake widths are in good agreement with the viscous core measurements, particularly the results of Dana and Short[7] and Murphy and Dickinson.[8] In the region $7 \gtrsim x/(C_DA)^{1/2} \lesssim 60$, the data of Slattery and Clay[5, 6] lie above the other results, whereas, for $x/(C_DA)^{1/2} < 7$, the luminous data appear to be somewhat larger than the shadowgraph and schlieren results.

If the temperature profiles across the wake are shrinking with distance downstream, once the threshold of sensitivity of a given instrument has moved into the viscous core, it will not reverse this trend and move back into the inviscid flow field. It is less obvious that this threshold does not lie inside the viscous core. There are several facts, however, that cause the contours of constant radiant power to increase

abruptly along the edge of the viscous core in the region of the wake characterized by small scale turbulence. First, the ablation products of lexan projectiles C_2, CN, and carbon particles[11, 21] are all much stronger radiators than air and are contained only in the viscous core. Secondly, the enthalpy or temperature profiles of the viscous core are probably relatively flat with very steep gradients at the edges of the core.[2] The presence of this relatively flat temperature profile means that lines of constant radiant power will move abruptly into the viscous core when the wake has cooled far downstream. Examination of the data from the wake scanner has verified the presence of the abrupt gradients in radiant intensity at the edges of the viscous core. Experience with the data from all three techniques showed that an abrupt decrease of the luminous width did indeed occur when the instrument thresholds were reached. It may be concluded, then, that the luminous widths observed correspond to the viscous core of the wake for $x/(C_DA)^{1/2} \gtrsim 7$ and as far back in the wake as the data presented herein extended ($x/(C_DA)^{1/2} \simeq 1200$).

The base and near wake region [$x/(C_DA)^{1/2} \lesssim 7$] is subject to several significant effects. First, in this region of the flow field, there is considerable radiation from the shock-heated inviscid flow field, in addition to that from the ablation products in the viscous flow. This conclusion is supported by examination of the present data (Fig. 1) and from similar results obtained at CARDE.[21] The extent of this radiation is strongly dependent on the projectile velocity (for a given shape) and the sensitivity of the instrument. The present experiments were directed primarily toward obtaining data over a long length of the wake rather than to establishing the details of the radiation profiles in the region about and just behind the body. Secondly, for 69 of the 77 rounds included in this composite luminous wake growth curve, the quasi-spherical projectile was employed, whereas spheres were used for the density gradient measurements. The entire flow field about the former body, and thus the initial enthalpy profiles and pressure in the near wake, is modified considerably by the increased bluntness and the cylindrical portion of this body compared to a spherical model. For example, the free shear layer is expected to have a smaller angle relative to the body axis than for a sphere, resulting in a wider viscous wake at the neck region. Also, the strength of the recompression shock is directly related to the flow turning angle, i.e., to the flow about the base of the body. As a result, the initial properties of the viscous core which determine its early growth[2] are subject to considerable variation with body shape. From these considerations, it should not be anticipated that the present luminous results for the quasi-spheres would show coincidence with density gradient measurements of the boundary-layer induced core for spheres in the near wake region.

Effect of Saboting

Since data have been taken with both saboted and unsaboted projectiles, it is of interest to see if there is any apparent effect of saboting on the luminous growth measurements. It is evident from Fig. 5 that the data for the 1.0-in.-diam saboted spheres are in excellent agreement with the measurements made with the 0.55-in.-diam unsaboted models. There is some experimental evidence obtained at CARDE[21] from absolute radiometric and spectroscopic measurements that the radiation intensity from wakes of saboted projectiles is less than from wakes of unsaboted projectiles under similar conditions of velocity and freestream pressure. However, it is not clear whether this effect is entirely due to the sabot launching technique since the saboted spheres were fired under much more closely controlled conditions of range purity and projectile cleanliness.

The unsaboted projectile will be friction heated in the gun barrel and may be at a higher temperature than the unsaboted model. However, it does not seem likely that this effect would change the wake growth since the only requirement to provide a concentration of luminous ablation products in the viscous wake is that ablation has begun at the measuring station. For the data reported here, the time to start ablation is calculated[22] to be much less than the flight time to the data-gathering stations on the range.

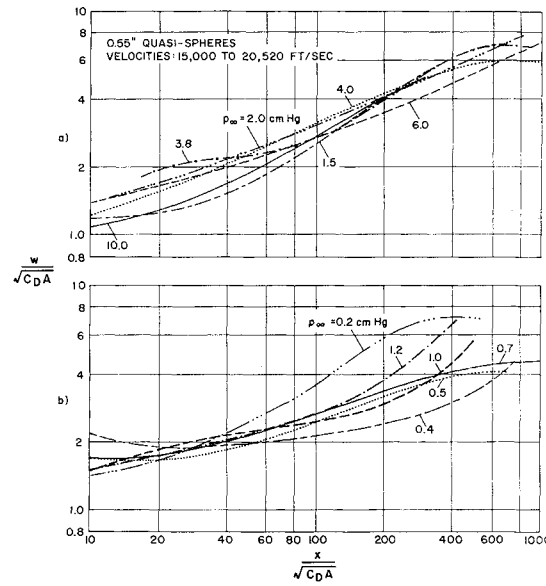

Fig. 7 Comparison of wake scanner data for various freestream pressures. In a, the composite quartic curve fits are shown for six pressures from 1.5 to 10 cm Hg where the wake is turbulent. In b, the curve fits are shown for six other pressures in the laminar and transition regimes, 0.2 to 1.2 cm Hg.

Freestream Pressure Effects

The effect of the freestream pressure or Reynolds number on the growth of the boundary-layer induced wake was investigated with data from the wake scanner obtained on the 0.55-in.-diam quasi-spherical body. Composite plots were formed from data at each of twelve pressures in the range $0.2 \leq p_\infty \leq 10.0$ cm Hg, which included velocities of 15,000 to 20,500 fps. The curve fits to the data at each pressure are shown in Fig. 7a for pressures sufficiently high so that the viscous wake is completely turbulent[23] and in Fig. 7b at pressures where the wake is in the laminar and transitional regime.

Figure 8 illustrates more clearly the pressure or Reynolds number dependence of the luminous wake growth data. The points are the average widths obtained from the curve fits to the data at 100, 200, and 400 $x/(C_DA)^{1/2}$ units downstream of the projectile. Interpolated values of the shadowgraph and schlieren data of other investigators[5-9] are also shown (see Fig. 6). The abscissa is the pressure parameter, $p_\infty (C_DA)^{1/2}$, suggested by Goldburg[23] for the correlation of wake transition for blunt bodies. The division into laminar and transitional or turbulent regimes is based on a transition Reynolds number at the shoulder of $R_{e_s} = 6000$, in agreement with the transition correlation of Fay and Goldburg.[9] The data of Figs. 7 and 8 indicate that for values of $p_\infty (C_DA)^{1/2} > 2.0$ cm Hg, where the wake is expected to be turbulent, the width of the boundary-layer induced wake is relatively insensitive to pressure. In the transition regime, $0.5 \leq p_\infty (C_DA)^{1/2} \leq 2.0$, the width appears to reach a minimum and then increases again in the laminar regime.

The solid curves on Fig. 8 show the pressure dependence of the wake width at $x/(C_DA)^{1/2} = 100$, 200, and 400 based on the diffusion relation[24]:

$$\frac{w}{(C_DA)^{1/2}} \propto \left[\frac{1}{(C_DA)^{1/2}}\right]^{1/2} \left[\frac{\nu(x/(C_DA)^{1/2}}{V_\infty}\right]^{1/2} \quad (1)$$

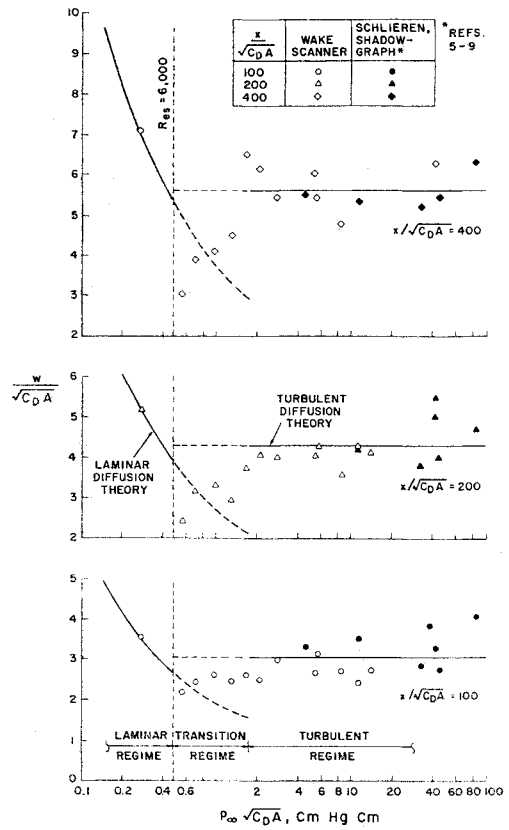

Fig. 8 Illustration of the pressure dependence of the luminous wake growth data and width data obtained with shadowgraph and schlieren techniques.

The diffusivities ν for laminar and turbulent flow, respectively, are given by

$$\nu_L = \mu/\rho = \mu RT/p \approx R(T)^{1.76}/p_\infty \quad (2)$$

$$\nu_T = w\Delta u/15 \quad (3)$$

where $p \approx p_\infty$ downstream of the expansion region and the Sutherland temperature dependence for the viscosity μ has been used for the laminar case. Using these relations, it can be seen that the laminar wake growth should have an inverse square root pressure dependence, whereas, in the turbulent regime, the growth is predicted to be independent of freestream pressure. In plotting Eq. (1) on Fig. 8, the constant of proportionality has been arbitrarily obtained from the data at $p_\infty(C_DA)^{1/2} = 0.275$ cm Hg-cm for the laminar condition and from the averaged data for $p_\infty(C_DA)^{1/2} \geq 2.00$ cm Hg-cm for the turbulent regime.

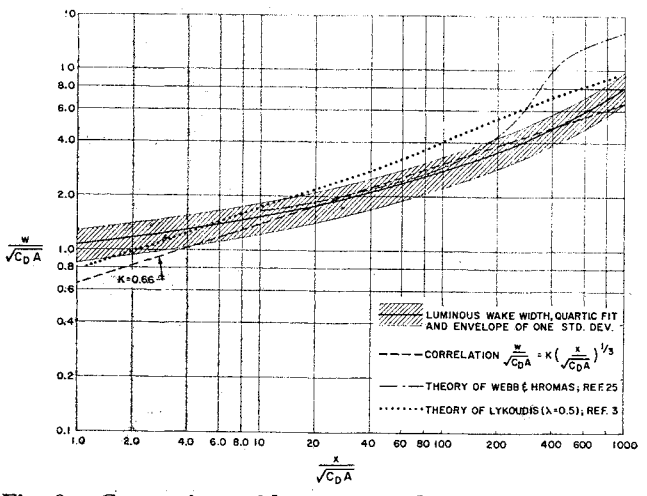

Fig. 9 Comparison of luminous wake growth data with various theoretical calculations.

The suggested pressure dependence is seen to be partially confirmed in Fig. 8. In the turbulent regime, both the present data and the shadowgraph and schlieren data of other investigators[5-9] indicate a width essentially independent of pressure over a factor of about forty in the parameter $p_\infty(C_DA)^{1/2}$. The inverse square root pressure dependence predicted for laminar wake growth is not established by the present data because of the lack of sufficient coverage at low pressures. In fact, the luminous data at the one pressure available well into the laminar regime indicates a stronger pressure dependence (more like $1/p$) although the scatter in the data precludes precise evaluation. It should be noted from Fig. 7 that this pressure effect is observed only for $x/(C_DA)^{1/2} \lesssim 60$, i.e., in the region where diffusion begins to dominate.

Comparison of Theory and Experiment

The results of these experiments are compared with various theoretical investigations in Fig. 9. The quartic fit of the turbulent luminous wake measurements is compared to theoretical results of Lees and Hromas[2, 20] and Lykoudis[3] and a semi-empirical correlation suggested by Fay.[24] Lees and Hromas developed a momentum integral method for the turbulent boundary-layer induced core that results in a numerical calculation for the wake width depending upon empirical results for the initial conditions and the turbulent diffusivity. The curve shown on Fig. 9 is a calculation by Webb and Hromas[25] of the growth of the viscous wake for the experimental conditions of $p_\infty = 6$ cm Hg and $V_\infty = 18{,}300$ fps., using initial conditions calculated to be appropriate for the 0.55-in.-diam projectile used in the experiments. As can be seen, the theory matches the experimental curve until about $x/(C_DA)^{1/2} \cong 200$ at which point the theory predicts a wake growth significantly greater than the data. This rapid growth in the theoretical curve takes place when the viscous core grows out into the region of large gradient of the inviscid enthalpy profile. It is interesting

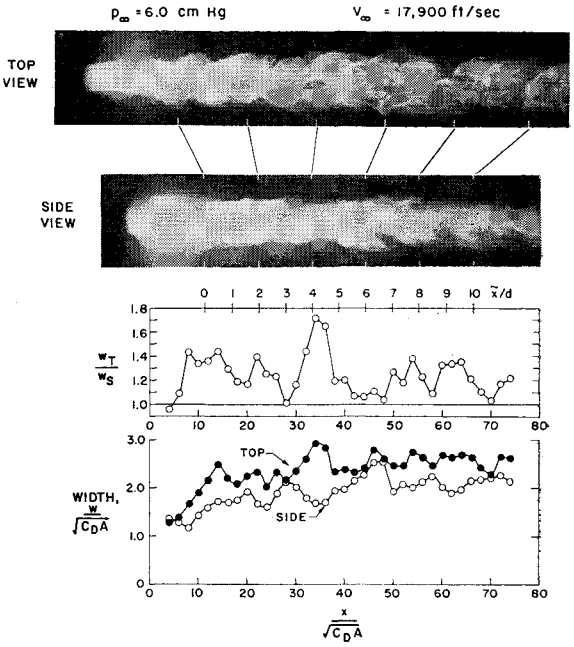

Fig. 10 Illustration of wake asymmetry. The race track photographs show the top view consistently larger than the side view. Because of a difference in the rotational velocity of the two recording drum cameras, the top view is not to the same axial scale as the side view. Direct correlation of events can be made by following the guide lines running between the photographs.

that the experimental data show no such effect out to at least 1000 body diameters.

Lykoudis[3] obtains a closed form solution for the wake growth incorporating the same physical considerations as Lees and Hromas. His results for $M_\infty = 16$ and $\lambda = 0.5$ for a sphere of $C_D = 1.0$ are also presented in Fig. 9. Good agreement with the luminous wake measurements is indicated for both the growth rate and the width, although the theoretical values in the range $x/(C_DA)^{1/2} \lesssim 40$ are somewhat above the experimental results. Consideration of the neck stagnation enthalpy scaling relation in Ref. 3 indicates a value of λ somewhat smaller than 0.5 would provide better agreement between the theory of Lykoudis and the present experiments. Lykoudis also considers the effects of Mach number variation. Unfortunately, the scatter of the present data (about 20%) exceeds the theoretical change in wake width of about 10% at $x/(C_DA)^{1/2} \simeq 100$ for a change of Mach number from 16 to 19.

For hypersonic wake growth for blunt bodies, Fay[24] suggests the use of the simple result of dimensional arguments:

$$w/(C_DA)^{1/2} = K[x/(C_DA)^{1/2}]^{1/3} \quad (4)$$

where $K = 0.9$. This semiempirical expression was fit to the present luminous wake growth data and the constant K determined to be 0.66 for values of $2 \leq x/(C_DA)^{1/2} \leq 1200$. The fit of Eq. (4) has an rms deviation of 23% compared to the deviation of 20% obtained with the quartic fit. It is concluded from the comparison of the quartic fit and the fit of Eq. (4) on Fig. 9 that a simple semiempirical expression, such as

$$w(C_DA)^{1/2} = 0.66[x/(C_DA)^{1/2}]^{1/3} \quad (5)$$

is adequate for prediction of the width of the luminous wake within the scatter of the data, although the rate of growth is not accurately predicted in some regions.

IV. Asymmetry of the Hypersonic Turbulent Wake

Photographs of the hypersonic turbulent wake have been recorded using two drum cameras mounted orthogonal to each other on the ballistic range. These two views of the wake, oriented at 90° from one another, allow the symmetry of the luminous wake to be determined. A total of 14 sets of pictures were obtained at $p_\infty = 6.0$ cm Hg for the 0.55-in.-diam projectile covering a velocity range of 16,600 to 18,600 fps. Two conclusions may be drawn from these data: 1) the luminous wake can be asymmetric or elliptical for much of its length, and 2) the asymmetries show an oscillation suggesting a large scale flow structure in the wake.

Typical data illustrating the first point are shown in Fig. 10. It is apparent from the race track photographs in this figure that the top view is wider than the side. Below the photographs, the ratio of the top to side widths, w_T/w_S, and also the actual width as a function of distance downstream in the wake have been plotted as obtained from the pictures. There are two scales used to plot the data: $x/(C_DA)^{1/2}$, the usual body-fixed coordinate system, and $\tilde{x}/d$, the local nondimensionalized distance between events in the wake which are tracked.**

The average value of the ratio of widths, w_T/w_S, was calculated for each of the 14 orthogonal runs by averaging the ratio measured every $2x/(C_DA)^{1/2}$ for the length of luminous wake available. This average ratio is plotted in Fig. 11 as the number of rounds within a certain range of asymmetry and illustrates the distribution of asymmetries. Although 14 cases are insufficient for a meaningful statistical study, it is apparent from Fig. 11 that the observed average

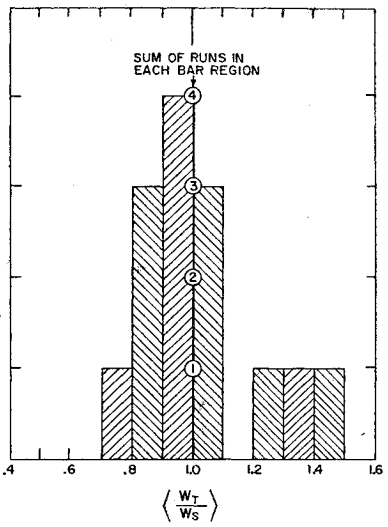

Fig. 11 Bar graph distribution of $\langle w_T/w_S \rangle$ for the 14 cases studied for asymmetry, where $\langle w_T/w_S \rangle$ represents the value of the top to side width ratio averaged over the entire length of race track data recorded in each case.

wake asymmetries suggest a random distribution centered around the symmetrical case $w_T/w_S = 1.0$.

The second observation of interest in this study is the interchange of the total wake width from top to side as one proceeds downstream in the wake, illustrated in Fig. 12. The scale of this phenomenon is about 1 to 2 $\tilde{x}/d$. This observation strongly suggests the presence of large scale eddies as proposed by Fay and Goldburg.[9]

The initial investigation of the symmetry of the turbulent hypersonic wake was carried out using a 0.55-in.-diam unsaboted quasi-sphere. Wake asymmetries could possibly have resulted from body angle of attack and rotation, and barrel heating. These phenomena were studied in Ref. 19 and found to be minimal in their effects on the observed wake asymmetry. Subsequent to these initial tests, a series of firings were conducted using a 1-in.-saboted lexan sphere to further verify these findings. Analysis of these results indicated similar asymmetries occurred, though noticeably subdued in length of ellipticity and amplitude of interweaving widths. The distribution of $\langle w_T/w_S \rangle$ for the saboted firings supports the initial results shown in Fig. 11 for the first test series.

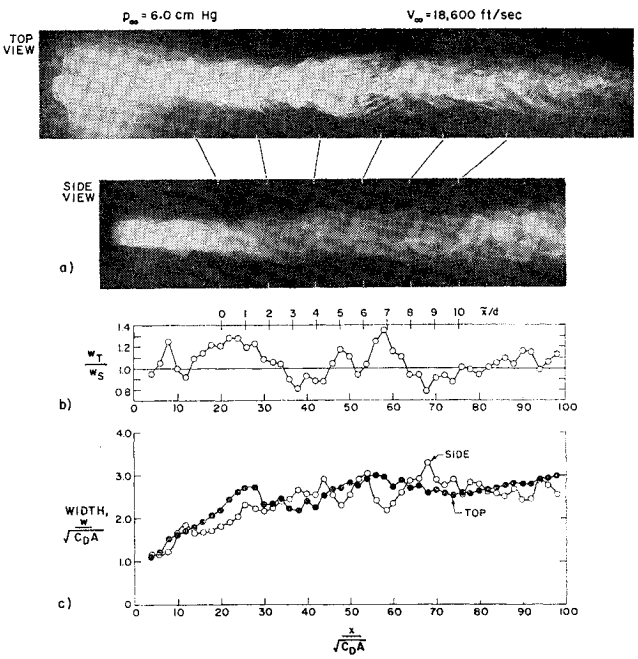

Fig. 12 Illustration of interweaving widths yielding an asymmetry that does not consistently remain oriented in one view.

** The scale x/d used here is the same as $(x/d)_{\text{film}}$ used in Ref. 16.

V. Summary

The results of this investigation of the luminous hypersonic wake may be summarized as follows:

1) It has been possible to measure the width of the luminous wake from the model out to about 1200 body diameters by the combined use of three techniques: image converter camera, race track camera, and wake scanner.

2) These luminous measurements are interpreted as defining the viscous boundary-layer induced core of the wake and are shown to agree with other shadowgraph and schlieren measurements of the width of the viscous core.

3) In the fully turbulent regime, the width was essentially independent of pressure; in the transition regime, the width was observed to reach a minimum; and for 0.2 cm Hg, where the wake should be laminar, the width was observed to increase again.

4) The turbulent theory of Lees and Hromas predicts a faster growth than the data beyond about 200 body diameters, whereas that of Lykoudis appears to give good agreement if the proper stagnation enthalpy at the neck is used. The simple asymptotic growth law can be made to fit the present data within the experimental uncertainty by an adjustment of the constant of proportionality from Fay's value of 0.9 to 0.66.

5) Photographs taken with two orthogonal race track cameras indicate significant asymmetries of the luminous unsteady hypersonic wake.

References

[1] Feldman, S., "On trails of axisymmetric hypersonic blunt bodies flying through the atmosphere," J. Aerospace Sci. **28,** 433–448 (1961).

[2] Lees, L. and Hromas, L., "Turbulent diffusion in the wake of a blunt-nosed body at hypersonic speeds," J. Aerospace Sci. **29,** 976–993 (1962).

[3] Lykoudis, P. S., "The growth of the hypersonic wake behind blunt and slender bodies," Rand Corp. RM-3270-PR (January 1963).

[4] Vaglio Laurin, R. and Bloom, M. H., "Chemical effects in external hypersonic flows," ARS Preprint 1976-61 (1961).

[5] Slattery, R. E. and Clay, W. G., "Width of the turbulent trail behind a hypervelocity sphere," Phys. Fluids **4,** 1199–1201 (1961).

[6] Slattery, R. E. and Clay, W. G., "Measurements of turbulent transition, motion, Statistics, and gross radial growth behind hypervelocity objects," Phys. Fluids **5,** 849–855 (1962).

[7] Dana, T. A. and Short, W. W., "Experimental studies of hypersonic turbulent wakes," General Dynamics/Convair Rept. Zph-103 (1961).

[8] Murphy, C. H. and Dickinson, E. R., "Growth of the turbulent wake behind a supersonic sphere," AIAA J. **1,** 339–342 (1963).

[9] Fay, J. A. and Goldburg, A., "The unsteady hypersonic wake behind spheres," ARS Preprint 2676-62 (1962).

[10] Hidalgo, H., Taylor, R. L., and Keck, J. C., "Transition in the viscous wakes of blunt bodies at hypersonic speeds," J. Aerospace Sci. **29,** 1306–1315 (1962).

[11] Lemay, A., "Radiation measurements from the plasma sheath surrounding hypersonic projectiles," Canadian Armament Research and Development Establishment TM 693/62 (March 1962).

[12] Magarvey, R. H. and Bishop, R. L., "Wakes in liquid-liquid systems," Phys. Fluids **4,** 800–805 (1961).

[13] Chippendale, R. A., "The photographic efficiency of image converters," *Proceedings of the Third International Congress on High-Speed Photography* (Academic Press, New York, 1956), pp. 116–125.

[14] Taylor, R. L., Keck, J. C., Washburn, W. K., Leonard, D. A., Melcher, B.W., II, and Carbone, R. M., "Techniques for radiation measurements and flow visualization of self-luminous hypersonic wakes," Avco-Everett Research Lab. AMP 84 (June 1962); also Transactions of the Seventh Symposium on Ballistic Missile and Space Technology (1962), Vol. 1, pp. 211–236.

[15] Tardiff, L., "Results obtained with an image converter camera in the study of radiation from hypersonic projectiles," Canadian Armament Research and Development Establishment TM 738/63 (January 1963).

[16] Washburn, W. K. and Keck, J. C., "Race track flow visualization of hypersonic wakes," ARS J. **32,** 1280–1282 (1962).

[17] Rinehart, J. S., Allen, W. A., and White, W. C., "Phenomena associated with the flight of ultra-speed pellets. Part III. General features of luminosity," J. Appl. Phys. **23,** 297–299 (1952).

[18] Taylor, R. L., Keck, J. C., Melcher, B. W., II, and Carbone, R. M., "A high speed scanner for transverse radiation measurements of luminous hypersonic wakes," AIAA J. **1,** 2186–2188 (1963).

[19] Taylor, R. L., Melcher, B. W., II, and Washburn, W. K., "Measurements of the growth and symmetry of the luminous hypersonic wake behind blunt bodies," Avco-Everett Research Lab. Res. Rept. 163 (May 1963).

[20] Hromas, L. and Lees, L., "Effect of nose bluntness on the turbulent hypersonic wake," Space Technology Labs. Rept. 6130-6259-KU-000 (October 1962).

[21] "Status report on the re-entry physics program, December 31, 1962," Canadian Armament Research and Development Establishment, TM 740/63 (April 1963).

[22] Brogan, T. R., "Electric arc gas heaters for re-entry simulation and space propulsion," ARS Paper 724-58 (1958).

[23] Goldburg, A., "Hypersonic wake transition," Avco-Everett Research Lab. Res. Note 393 (to be published).

[24] Fay, J. A., "A review of laboratory experiments on hypersonic wakes," ARS Reprint 2660-62 (1962).

[25] Webb, W. and Hromas, L., private communication (June 1964).